Detailed Chemical Characterization of Unresolved Complex Mixtures (UCM) in Atmospheric Organics: Insights into Emission Sources, Atmospheric Processing and Secondary Organic Aerosol Formation

Arthur W. H. Chan[1], Gabriel Isaacman[1], Kevin R. Wilson[2], David R. Worton[1,3], Chris R. Ruehl[1], Theodora Nah[4], Drew R. Gentner[5], Timothy R. Dallman[5], Thomas W. Kirchstetter[5,6], Robert A. Harley[5,6], Jessica B. Gilman[7,8], William C. Kuster[8], Joost A. de Gouw[7,8], John H. Offenberg[9], Tadeusz E. Kleindienst[9], Ying H. Lin[10], Caitlin L. Rubitschun[10], Jason D. Surratt[10], and Allen H. Goldstein[1,5,6]

[1]*Department of Environmental Science, Policy, and Management, University of California, Berkeley, CA, USA*

[2]*Chemical Sciences Division, Lawrence Berkeley National Laboratory, Berkeley, CA, USA*

[3]*Aerosol Dynamics Inc., Berkeley, CA, USA*

[4]*Department of Chemistry, University of California, Berkeley, CA, USA*

[5]*Department of Civil and Environmental Engineering, University of California, Berkeley, CA, USA*

[6]*Environment Energy Technologies Division, Lawrence Berkeley National Laboratory, Berkeley, CA, USA*

[7]*Cooperative Institute for Research in the Environmental Sciences (CIRES), University of Colorado, Boulder, CO, USA*

[8]*NOAA Chemical Sciences Division, Boulder, CO, USA*

[9]*National Exposure Laboratory, Office of Research and Development, Environmental Protection Agency, Research Triangle Park, NC, USA*

[10]*Department of Environmental Sciences and Engineering, Gillings School of Global Public Health, University of North Carolina at Chapel Hill, NC, USA*

A. W. H. Chan, D. R. Gentner, A. H. Goldstein, G. Isaacman, C. R. Ruehl, and D. R. Worton, Department of Environmental Science, Policy, and Management, 250 Hilgard Hall, University of California, Berkeley, CA 94720, USA. (arthurchan@berkeley.edu; ahg@berkeley.edu)

T. R. Dallmann and R. A. Harley, Department of Civil and Environmental Engineering, 760 Davis Hall, University of California, Berkeley, CA 94720, USA.

J. A. de Gouw, J. B. Gilman and W. C. Kuster, NOAA ESRL & CIRES, 325 Broadway CSD7, Boulder, CO 80305, USA.

T. W. Kirchstetter, Lawrence Berkeley National Laboratory, 1 Cyclotron Road, MS 70-108B, Berkeley, CA 94720, USA.

T. E. Kleindienst, J. H. Offenberg, National Exposure Research Laboratory, U.S. Environmental Protection Agency, Research Triangle Park, NC 27711, USA.

Y. H. Lin, C. L. Rubitschun, and J. D. Surratt, Campus Box 7431, University of North Carolina at Chapel Hill, Chapel Hill, NC 27599, USA.

T. Nah and K. R. Wilson, Lawrence Berkeley National Laboratory, 1 Cyclotron Road, MS 6R21, Berkeley, CA 94720, USA.

Abstract

Recent studies suggest that semivolatile organic compounds (SVOCs) are important precursors to secondary organic aerosol (SOA) in urban atmospheres. However, knowledge of the chemical composition of SVOCs is limited by current analytical techniques, which are typically unable to resolve a large number of constitutional isomers. Using a combination of gas chromatography and soft photoionization mass spectrometry, we characterize the unresolved complex mixture (UCM) of aliphatic hydrocarbons observed in Pasadena, CA (~16 km NE of downtown Los Angeles) and Bakersfield, CA during CalNex 2010. Knowledge of molecular structures, including carbon number, alkyl branching, and number of rings, provides important constraints on the rate of atmospheric processing, as the relative amounts of branched and linear alkanes are shown to be a function of integrated exposure to hydroxyl radicals. Emissions of semivolatile branched alkanes from fossil-fuel related sources are up to an order of magnitude higher than those of linear alkanes, and the gas-phase OH rate constants of branched alkanes are ~30% higher than their linear isomers. Based on a box model considering gas/particle partitioning, emissions and reaction rates, semivolatile branched alkanes are expected to play a more important role than linear alkanes in photooxidation of the UCM and subsequent transformations into SOA. Detailed speciation of semivolatile compounds therefore provides essential understanding of SOA sources and formation processes in urban areas.

Introduction

Organic matter represents a major fraction of ambient aerosol. A large fraction of organic aerosol (OA) is formed from oxidation of gas-phase hydrocarbons, and is known as secondary organic aerosol (SOA) [*Zhang et al.*, 2007]. However, current atmospheric models typically underestimate the budget of SOA, highlighting a lack of understanding in the sources and

transformation processes of organic compounds in the atmosphere [*Goldstein and Galbally*, 2007]. Recently, it has been proposed that oxidation of semivolatile organic compounds (SVOCs) is a major source of SOA, particularly in urban atmospheres [*Pye and Seinfeld*, 2010; *Robinson et al.*, 2007]. SVOCs are defined as compounds which have effective saturation concentrations (C^*) between 0.1 and 10 μg m^{-3}. Owing to the low vapor pressures of SVOCs and of their subsequent reaction products, oxidation of SVOCs is expected to have significantly higher SOA yields than more volatile precursors, and, despite lower emissions, could dominate SOA formation in urban areas. Models that incorporate transformations of SVOCs to SOA yield better predictions of the total amount of SOA and its seasonal variability [*Hodzic et al.*, 2010; *Robinson et al.*, 2007]. However, these models tend to underestimate the observed O/C ratios, and fail to capture the diurnal variations [*Hodzic et al.*, 2010] and vertical profiles of SOA [*Heald et al.*, 2011], suggesting that the atmospheric chemistry of SVOCs leading to SOA formation is poorly understood. Their relative oxidation rates and mechanisms, the two key factors that determine the amount and properties of SOA formed, are currently extrapolated from those of smaller carbon numbers.

Detailed knowledge of the identities and chemistry of semivolatile compounds is challenging, as the chemical composition is highly complex and current analytical techniques are unable to separate and identify these compounds. While gas chromatography-mass spectrometry (GC/MS) has been the most common method for speciating these compounds, atmospheric sources often emit a large number of compounds, which cannot be separated by traditional GC methods. As a result, many atmospheric samples contain a large unresolved peak in chromatographic analyses, often referred to as the unresolved complex mixture (UCM) [*Schauer et al.*, 1999]. The UCM

can account for more than 80% of semivolatile emissions from diesel [*Schauer et al.*, 1999] and gasoline engines [*Schauer et al.*, 2002], representing a major fraction of SVOCs in urban areas [*Williams et al.*, 2010b]. Furthermore, the UCM is ubiquitous in environmental chemistry, often found in samples associated with fossil fuel use [*Frysinger et al.*, 2003; *Nelson et al.*, 2006; *Ventura et al.*, 2008].

The UCM is thought to contain a large number of constitutional isomers, most of which are linear (also termed straight-chained or normal), branched, or cyclic alkanes [*Mao et al.*, 2009]. In contrast, aromatic compounds comprise only a minor fraction of the UCM [*Van Deursen et al.*, 2000]. Owing to the challenges in speciating alkane isomers, SVOCs have typically been classified by volatility only, inferred from thermodenuder measurements or gas chromatography retention times [*Grieshop et al.*, 2009; *Presto et al.*, 2012], which then serve as inputs into the aforementioned models [*Hodzic et al.*, 2010; *Pye and Seinfeld*, 2010]. Information about molecular structures is generally overlooked. However, the number of rings and alkyl branches in alkanes strongly affect their oxidation chemistry and their SOA yields [*Lim and Ziemann*, 2009; *Tkacik et al.*, 2012]. Molecular structure also plays an important role in other degradation pathways of environmentally relevant complex mixtures [*Nelson et al.*, 2006]. As a result, knowledge of molecular structure is crucial to understanding the sources and environmental fate of these hydrocarbons.

The main objective of this work is to characterize the molecular composition of ambient UCM, classify the components by molecular structure for use in future models of urban atmospheres, and use this detailed information to understand their atmospheric processing and SOA formation.

Previously, we have demonstrated that constitutional isomers present in diesel fuel can be characterized using gas-chromatography coupled to vacuum ultraviolet ionization mass spectrometry (GC/VUV-MS) [*Isaacman et al.*, 2012a]. We combine this technique with comprehensive 2-dimensional gas chromatography (GC×GC/VUV-HR-TOFMS) to characterize in detail the composition of ambient semivolatile compounds observed during the California Research at the Nexus of Air Quality and Climate Change (CalNex) campaign in summer 2010. The samples were collected at two urban sites in California (Pasadena, CA and Bakersfield, CA). Using detailed speciated measurements of linear, branched and cyclic alkanes in the UCM, we constrain their relative oxidation rates and provide valuable insights into their sources, processing and relative contributions to SOA formation. The utility of the analytical technique in resolving aliphatic, aromatic and polar species observed in the ambient atmosphere is also discussed.

Methods

Sampling locations

The samples described in this manuscript were collected at two urban sites in California (Pasadena, CA and Bakersfield, CA) as part of the CalNex field campaign in the summer of 2010 (www.esrl.noaa.gov/csd/calnex/). Pasadena sampling was conducted on the campus of the California Institute of Technology, ~16 km NE of downtown Los Angeles (hereafter referred to as the LA site). Two $PM_{2.5}$ samples from the LA site, collected on Sunday May 30 (3:00 – 6:00 PM local time) and Saturday June 5 (midnight – 11 PM local time), were selected for analysis under VUV ionization, as these two days represented different degrees of photochemical aging, the significance of which will be discussed below. 54 samples from the intensive filter sampling

periods, collected at a time resolution of 3 to 6 hours, were analyzed under electron impact (EI) ionization. Sampling at the Bakersfield site was conducted at the southeast edge of the city, co-located with other instruments participating in the field campaign. Two 23-hour samples, collected on Friday June 18 and Wednesday June 23 from midnight to 11 PM local time, were selected for VUV analysis. These two samples, along with 32 other daily (midnight – 11 PM) filter samples were also analyzed under EI. All samples collected from the Pasadena site were collected on quartz fiber filters (Tissuquartz™ Filters, 2500 QAT-UP, Pall Life Sciences), which were 20 cm × 25 cm, allowing for high-volume $PM_{2.5}$ sampling at ~1 m^3 min^{-1}. All samples collected from the Bakersfield site were collected on 86 cm^2 quartz fiber filters (Pall Life Sciences); however, medium-volume $PM_{2.5}$ sampling at 226 L min^{-1} was conducted. All filters were pre-baked at 550 °C to remove any organic contaminants. Filter samples were stored in a freezer at −18 °C until chemical analysis. Field blanks were collected every 7–10 days by placing a pre-fired quartz fiber filter into the sampler for 15 min before removing and storing in the same manner as the field samples. Analysis of both field and laboratory blanks showed no significant aliphatic contaminants on pre-fired quartz filters.

Additional samples collected during a study conducted at the Caldecott Tunnel in Oakland, CA were also analyzed for comparison [*Dallmann et al.*, 2012]. Here we focus our analysis on 2 weekday filter samples collected in the gasoline-only bore, and 5 samples collected in the mixed gasoline/diesel bore (4 weekday and 1 weekend samples). Emissions during collection of the 2 weekday samples from the gasoline-only bore and the weekend sample from the mixed bore are expected to be dominated by gasoline vehicles (3 “gasoline-dominated'” samples), while emissions during the 4 weekday samples in the mixed bore are expected to be dominated by

diesel vehicles (4 “diesel-dominated” samples). In addition to thermal desorption of filter samples, SAE 10W-30 motor oil and 3 samples of crude oil extracted and refined in the San Joaquin Valley region were also analyzed for their chemical composition. The origins of the crude oil samples are confidential for proprietary reasons.

Speciation of semivolatile hydrocarbons

Selected samples were analyzed using comprehensive 2-dimensional gas chromatography coupled to a vacuum-ultraviolet high-resolution time-of-flight mass spectrometer (GC×GC/VUV-HRTOFMS). Filter punches (total area of 1.6 cm^2) were thermally desorbed at 320 °C under helium using a thermal desorption system and autosampler (TDS3 & TDSA2, Gerstel). Desorbed samples were focused at 20 °C on a quartz wool liner in a cooled injection system (CIS4, Gerstel) before they were introduced into a gas chromatograph (GC, Agilent 7890). For motor oil and crude oil, samples diluted in chloroform were directly injected via a septumless inlet into the GC.

Comprehensive GC×GC was performed using a 60 m × 0.25 mm × 0.25 µm non-polar capillary column (Rxi-5Sil MS, Restek) for the first-dimension separation (by volatility), and a medium-polarity second dimension column (1 m × 0.25 mm × 0.25 µm, Rtx-200MS, Restek). A dual-stage thermal modulator (Zoex), consisting of a guard column (1 m × 0.25 mm, Rxi, Restek), was used as the interface between the two columns, where the effluent from the first column was cryogenically focused and periodically heated for rapid transfer into the second column. The modulation period was 2.4 seconds.

Effluent from the second column was analyzed using a high-resolution (m/Δm ~ 4000) time-of-flight mass spectrometer (HTOF, Tofwerk) coupled to the Advanced Light Source at Lawrence Berkeley National Laboratory. Single photon ionization by the vacuum ultraviolet (VUV) beam used here is similar to that reported previously [*Isaacman et al.*, 2012a]. In brief, photons of 10.5 eV with an energy distribution width of 0.2 eV and an intensity of ~10^{15} photons s^{-1} were generated by the Chemical Dynamics Beamline (9.0.2). The photon beam was introduced orthogonally to the GC effluent, and ionized molecules were accelerated into the extraction region. Since the ionization energies of most organic compounds are between 8 and 11 eV, the minimal excess energy (compared to electron impact ionization at 70 eV) limits fragmentation of ionized molecules, allowing for significant detection of the molecular ions ($M^{\bullet+}$). The ion chamber was maintained at 150 °C to minimize fragmentation. All LA and Bakersfield samples were also analyzed under EI at 70 eV, using a standard tungsten filament.

The molecular ion signals for linear, branched and cyclic alkanes under VUV ionization are used as the basis for quantification [*Isaacman et al.*, 2012b]. Details about the calibration method based on molecular structures are described in Appendix A of the Supplementary Material. The adjusted molecular ion signals were then quantified based on known quantities (5 ng each) of perdeuterated internal standards (*n*-hexadecane-d_{34}, *n*-eicosane-d_{42}, *n*-tetracosane-d_{50}, and *n*-octacosane-d_{58}, C/D/N Isotopes) spiked onto the filter punches prior to analysis. In quantifying the aliphatic hydrocarbons, only the UCM region of the chromatogram was considered (second dimension retention time between 0.4 and 0.9 seconds). Polycyclic aromatic hydrocarbons (PAHs) and highly oxygenated compounds are not expected to elute in this region. In addition, signals of oxygen-containing molecular ions were removed by high-mass-resolution data

processing procedures [*Isaacman et al.*, 2012b], such that only aliphatic molecular ions ($C_xH_y^+$) were considered for quantification. All data processing and visualization of GC×MS data were performed using custom code written in Igor 6.2.2 (Wavemetrics), while visualization of 2-dimensional chromatography data and detection of chromatographic peaks were carried out using GC Image software (LLC).

Other measurements

Co-located measurements of volatile organic compounds (VOCs) by *in situ* GC/MS are also used for comparison. Details of the GC/MS technique used in LA are described by *Gilman et al.* [2010]. Average photochemical age of air masses at the LA site was calculated using the ratio of 1,2,4-trimethylbenzene to benzene [*Borbon et al.*, 2012; *Parrish et al.*, 2007]. GC/MS measurements of light hydrocarbons at the Bakersfield site were used for source identification purposes. Details of the GC/MS technique are described by *Gentner et al.* [2012].

Results and Discussion

Resolving the UCM using GC×GC and GC×MS

Figure 1 shows the total integrated ion chromatogram of the LA and Bakersfield samples under VUV ionization. Similar to previous work using GC×GC to analyze atmospheric samples, PAHs and oxygenated compounds, such as acids and ketones, are readily separated from aliphatic compounds [*Worton et al.*, 2012]. Examples of these peaks are provided in Fig. S-2 in the Supplementary Material. Despite the increased peak capacity, there is still a large unresolved "hump" in the nonpolar region of the chromatogram, representing the UCM. The dominance of the UCM is present in most ambient samples that were analyzed by EI. The inability of GC×GC

to resolve these aliphatic hydrocarbons is likely due to the large number of possible constitutional isomers [*Goldstein and Galbally*, 2007], resulting in overlapping volatilities. In addition, even though the isomers are structurally different, all hydrocarbons are nonpolar and are essentially unretained in a polar column, resulting in poor second-dimension resolution. Further chromatographic separation of the UCM can be performed using other column pairings [*Nelson et al.*, 2006], reversed-phase chromatography [*Vogt et al.*, 2007], or coupled liquid chromatography-GC×GC [*Mao et al.*, 2009]. However, in analyzing atmospheric samples, a polar column is preferred owing to the need for also separating aromatic and oxygenated compounds which are prevalent. Orthogonal separation by volatility and polarity also allows for convenient inputs into 2-dimensional frameworks used to model evolution of organic compounds in the atmosphere [*Isaacman et al.*, 2011; *Jimenez et al.*, 2009].

In this work, the aliphatic UCM is characterized by a novel method using a combination of gas chromatography and soft VUV photoionization. Traditional GC/MS employs electron impact at 70 eV as the ionization technique, which imparts a large amount of excess energy and causes extensive fragmentation. While the fragmentation mass spectra can in many cases be useful for compound identification, aliphatic compounds have almost identical fragmentation patterns, with a large fraction of signal at *m/z* 41, 43, 55, 57, 69, 71 etc. (corresponding to $C_xH_{2x+1}^+$ and $C_xH_{2x-1}^+$ ions, where *x* is typically between 3 and 6). As a result, these compounds cannot be distinguished from each other, as illustrated in Fig. 2a. Soft ionization retains the identity of a molecule by maximizing the relative signal of the molecular ion, albeit at the loss of ionization efficiency. Similar to aliphatic compounds in diesel fuel shown in our previous study, coupling soft ionization with volatility-based GC separation allows hydrocarbons in the UCM in the ambient

atmosphere to fall into distinguishable patterns in a GC×MS plot (Fig. 2b) [*Isaacman et al.*, 2012a; *Wang et al.*, 2005].

In the GC×MS diagram, each cluster corresponds to a carbon number. Within each carbon number, the molecular formulas can be identified from molecular weights of parent ions, shown on the y-axis. As a result, the complex mixture can be speciated by number of carbon atoms and the number of double bond equivalents, N_{DBE}, which is the total number of rings and C=C double bonds. In the samples from both urban sites, the observed UCM lies in the range of 20 to 25 carbon atoms. In this range, alkanes have saturation vapor pressures between 9×10^{-8} and 9×10^{-6} torr (saturation concentrations between approximately 2 μg m^{-3} and 200 μg m^{-3} at 298K), and are therefore semivolatile and expected to exist in both the particulate and gas phases under atmospheric loadings [*Williams et al.*, 2010a]. It must be noted that smaller, more volatile hydrocarbons are expected to be abundant, but cannot be effectively and quantitatively collected on quartz filter samples used in this study. Most hydrocarbons observed have $N_{DBE} < 6$. Alkenes in this molecular weight range are highly reactive and are not expected to be significant in atmospheric samples. While alkene production from thermal decomposition of labile compounds (containing oxygen or nitrogen) cannot be ruled out, the distributions across different N_{DBE} classes were similar to those observed in unoxidized motor oil [*Isaacman et al.*, 2012b]. Therefore, cyclic alkanes (not alkenes) are expected to dominate aliphatic compounds observed with $N_{DBE} > 0$ in Bakersfield and LA, similar to alkanes found in motor oil.

Within each DBE class, gas chromatography provides separation of isobaric compounds (with the same molecular formula) by volatility. Since branched alkanes are more volatile than their

linear counterparts of the same carbon number, they elute earlier relative to the respective linear alkane from the first dimension column. As shown in Fig. 2c, good chromatographic resolution is achieved for linear and branched alkanes with N_{DBE} = 0. Unlike in diesel fuel [*Isaacman et al.*, 2012a] but as observed in motor oil [*Isaacman et al.*, 2012b], structural isomers are not well resolved for N_{DBE} > 0. This is most likely due to the higher carbon number range of the ambient UCM, and, hence, a greater number of possible *E/Z* configurations. As a result, mass concentrations of branched isomers are only reported for acyclic alkanes (N_{DBE} = 0). Following the naming convention of our previous work, we refer to branched isomers which contain *x* alkyl branches as B*x* isomers. For example, B0 refers to the linear alkane, B1 refers to alkanes with 1 alkyl branch etc.

To the authors' knowledge, this work represents the most detailed characterization of the UCM in atmospheric samples to date. The calibrated masses of linear, branched and cyclic alkanes for carbon numbers between 20 and 25 are shown in Fig. 3. The relative ratios of total branched alkanes to linear alkanes (hereafter referred to as B/N ratio) vary greatly between the two urban sites, from ~1 in the June 5 LA sample to >10 in both Bakersfield samples, shown in Fig. 4.

Processing of semivolatile hydrocarbons in Los Angeles, CA

In both LA samples analyzed under VUV photoionization, while the unresolved "hump" is visible in the chromatogram, aromatic and more polar compounds have a higher total integrated ion signals than the UCM (Fig. 1a). The most abundant isomer for each carbon number is the linear alkane, accounting for >30% of the total acyclic alkane mass. The two samples analyzed under VUV represent two different periods in the field campaign. From June 2 through June 6,

there was a steady build-up of pollutants due to periodic entrainment of the residual layer aloft, causing fresh emissions in the boundary layer to be mixed with aged pollutants that remained in the basin [*Pollack et al.*, 2012]. On May 30, no such build-up was observed. Owing to this difference in meteorological conditions, the integrated OH exposure, calculated from the ratios of 1,2,4-trimethylbenzene (1,2,4-TMB) to benzene [*Borbon et al.*, 2012], was higher during collection of the June 5 sample (4.8×10^{10} molec cm^{-3} s) than that of the May 30 sample (2.6×10^{10} molec cm^{-3} s).

The B/N ratios of C_{21}–C_{24} hydrocarbons in the May 30 sample are higher than those in the June 5 sample, suggesting that branched alkane isomers are consumed more rapidly relative to the linear isomers of the same carbon number. Since the aliphatic hydrocarbons in the UCM are predominantly saturated, their primary sink in the atmosphere is reaction with OH radicals. Although compounds in this volatility range exist in both the gas and particle phases, C_{21}–C_{24} hydrocarbons are sufficiently volatile that their gas phase reactions with OH are dominant over particle-phase reactions at ambient levels of OA concentrations [*Lambe et al.*, 2009]. We therefore expect that the change in B/N ratios is primarily a result of differences in gas-phase reaction rates with OH radicals, and the decay can be described by the following equation:

$$\left(\frac{B}{N}\right)_{sample} = \left(\frac{B}{N}\right)_0 e^{(k_N f_N - k_B f_B)\int[OH]dt} \quad (1)$$

where $(B/N)_0$ is the B/N ratio at the source; $(B/N)_{sample}$ is the B/N ratio of each individual sample; k_B is the average OH reaction rate of all branched isomers (cm^3 $molec^{-1}$ s^{-1}), which is treated here as an unknown; k_N is the OH reaction rate of the linear alkane (cm^3 $molec^{-1}$ s^{-1}), calculated from structural-reactivity relationships [*Kwok and Atkinson*, 1995]; f_N is the average gas-phase fraction of the linear isomer; f_B is the average gas-phase fraction of branched isomers,

and $\int [OH] dt$ is the integrated OH exposure (molec cm^{-3} s) for that sample, calculated from the 1,2,4-TMB to benzene ratios [*Borbon et al.*, 2012]. Equation (1) is similar in form to previous investigation of hydrocarbons clocks for gas-phase oxidation, with one notable exception. Here we include the effect of gas-particle partitioning, which reduces the fractions of alkane species in the gas phase available for OH reactions. The gas-phase fraction for each filter data point is calculated individually based on known vapor pressures [*Pankow and Asher*, 2008; *Williams et al.*, 2010a], total OA mass concentrations measured by the Aerodyne Aerosol Mass Spectrometer (AMS) and temperature. Both OA mass concentrations and temperatures were similar between the two filter sampling periods (at 7 μg m^{-3} and 290K). For the data shown in Fig. 5, we assume that f_N and f_B are constant in order to derive k_B for each carbon number.

To investigate the relationship between B/N ratios and OH exposure, the B/N ratios at the source (corresponding to zero OH exposure) must be known. Since the major contributor of hydrocarbons in the LA Basin is likely motor vehicles [*Williams et al.*, 2010b], the B/N ratios of hydrocarbons in the LA ambient samples are compared to those in fresh vehicular exhaust, measured during a tunnel study in Oakland, California. Here we focus on the branched and linear acyclic alkanes between C_{21} and C_{24}. The average B/N ratios of these alkanes in all 7 tunnel samples are presented in Fig. 4. There were no systematic differences in B/N ratios between diesel-dominated and gasoline-dominated samples in this carbon number range, so here we report the standard deviation in the 7 samples to be the uncertainty in B/N ratios for each carbon number. The average B/N ratios observed in these tunnel samples, which are higher than those observed in the LA samples, serve as additional data points corresponding to zero OH exposure at the source. Assuming that the decrease in B/N ratio is entirely due to photooxidation, the

relative reaction rates of the branched isomers can be estimated from the decay of B/N ratios. A plot of B/N ratio versus OH exposure is shown in Fig. 5. From regression using equation (2), a value for k_B for each carbon number can be derived from the slope of the best-fit line ($f_N k_N - f_B k_B$). In general, the average rate constants of branched alkane isomers are 21–35 % higher than that of the linear alkanes (see Table 1).

The uncertainties in the regressions on the B/N ratios measured using VUV are considerable, owing to the limited number of samples analyzed using this technique. To further constrain the dependence of B/N ratios on photochemical processing, analysis of samples covering a wide range of photochemical processing is needed. As mentioned before, under electron impact, detailed speciation, similar to that achieved in Fig. 3, is difficult owing to extensive fragmentation and co-elution of isomers. However, some B0 (linear) and B1 isomer peaks can be resolved from other isomers, and their retention times and molecular formulas are confirmed by VUV analysis, as shown in Fig. 6. Each linear isomer coelutes with a B2 isomer with one more carbon atom, but, based on observations from VUV, this B2 isomer is expected to contribute <15% of the total ion signal for C_{22}–C_{24} alkanes in the LA samples. Other isomers, such as B2 isomers and isomers with $N_{DBE} > 0$ remain unresolved under EI. The ratio of B1 to linear isomers (B1/N ratios) for each carbon number was calculated from the background-subtracted signals on $C_4H_9^+$ (*m/z* 57), the most common alkane fragment ion. Using this method, more reliable estimates of k_B are derived from EI data, which consist of a larger number of samples. However, temperature and OA mass can no longer be assumed to be constant, and these factors critically determine gas-phase fractions and hence oxidation rates of SVOCs. For the EI data set, we first determine the average photochemical age for each sample, assuming an [OH] of 2×10^6 molec

cm^{-3}. An average temperature and OA mass, to which each air plume represented by the sample has been exposed, are then determined. With this information, a B1/N ratio for each sample can be calculated for any given k_{B1} and $(B1/N)_0$ using Equation (1), and optimal values for these two parameters are determined that minimizes the absolute error between calculated and observed B/N ratios derived from EI data. The regressions are shown in Fig S-3 in the Supplementary Material. Values for k_{B1} are consistent with those derived from VUV data, as shown in Table 1, confirming that B1 isomers of C_{22}–C_{24} alkanes are consumed more rapidly than linear isomers. Figures 7a–7c show the diurnal profiles of the B1/N ratios, and the minima in B1/N ratios occur between late morning and early afternoon. The daytime minima are likely a result of higher OH concentrations and greater extent of oxidation. In a later section, we will rule out higher daytime temperatures (which alters gas/particle partitioning) to be the cause of the observed drop in B1/N ratios.

Structure-reactivity predictions for linear and branched alkanes with 21 to 24 carbons are summarized in Table 1. The predicted rate constants of branched alkanes are 1–8% higher than those of the linear isomers, lower than the ratios observed. Under these predictions, a combination of a tertiary and a primary carbon atom have higher OH reaction rates than two secondary carbon atoms if the tertiary carbon atom is not at the 2-position [*Kwok and Atkinson*, 1995]. While small ($<C_5$) branched hydrocarbons have lower OH rate constants than their linear isomers, it is more statistically likely for C_{21}–C_{24} alkanes that alkyl branching will instead occur at the 3- or higher positions, resulting in higher predicted OH rate constants. It is also noteworthy that preferred depletion of branched isomers was also observed during experimental studies of heterogeneous oxidation of motor oil particles [*Isaacman et al.*, 2012b]. In those experiments,

oxidation is expected to occur in the particle phase owing to the high particulate loadings, and the ratios of the rate constants (k_B/k_N = 1.28) reported are roughly consistent with those of gas-phase rate constants observed in this work.

While the possibility of additional sources with low B/N ratios cannot be ignored, differences in this ratio caused by some potential primary sources of aliphatic hydrocarbons can be ruled out. There is no odd carbon preference in this range of carbon numbers, indicating that plant wax is not a major contributor to aliphatic compounds in the UCM. Also, wood burning markers, such as dehydroabietic acid and retene, were not observed at significant concentrations, indicating that the trend in B/N ratios is not caused by emissions of linear alkanes from biomass or biofuel burning. No additional source of linear alkanes contributing to the lower B/N ratios in more aged samples has yet been identified. We also considered whether the changes in B/N ratio could be caused by a difference in fleet between Oakland, CA and the LA Basin, but concluded that differences would likely be minimal across the state. Additionally, this would only affect B/N ratios of the emission source $(B/N)_0$, and would be unlikely to cause B/N ratios to decrease with photochemical age as demonstrated.

Source of semivolatile hydrocarbons in Bakersfield, CA

Semivolatile and non-volatile hydrocarbons in Bakersfield appear to originate from a broader combination of sources than in LA. First, the high concentrations of odd-number *n*-alkanes (C_{23} and C_{25}, see Fig. 3d) suggest that plant wax could be a major source. The carbon number preference index (CPI) of *n*-alkanes between C_{21} and C_{33} is given by the following equation [*Marzi et al.*, 1993]:

$$CPI = \frac{\sum_{i=10}^{15} C_{2i+1} + \sum_{i=11}^{16} C_{2i+1}}{2\sum_{i=10}^{15} C_{2i}} \quad (2)$$

where C_x is the concentration of *n*-alkanes with *x* carbon atoms. The CPI of Bakersfield samples were consistently above 2, indicating a strong contribution of plant wax. In contrast, the average CPI of LA samples were below 1.4. This is consistent with factor analysis using AMS and FTIR data from CalNex Bakersfield, which suggests that up to 10% of organic aerosol is likely vegetative detritus [*Liu et al.*, 2012].

Using GC/VUV, the alkane isomers in the UCM are classified into branched, cyclic and linear alkanes based on molecular weights and GC retention times. Branched isomers dominate over linear isomers in Bakersfield, with B/N ratios greater than 10. These B/N ratios are inconsistent with those measured in the LA samples, and are even higher than those observed in fresh motor vehicle exhaust from the tunnel samples. Since semivolatile branched alkanes react with OH radicals faster than linear isomers both theoretically (from structure-reactivity relationships) and in flow tube experiments [*Isaacman et al.*, 2012b], photochemical processing is not expected to increase the B/N ratios from those of motor vehicle UCM to those observed in Bakersfield. While factor analysis of particle-phase molecular markers suggest that a major source of linear alkanes is motor vehicles [*Zhao et al.*, 2012], the high B/N ratio of the UCM suggests that there is a also large source of predominantly branched semivolatile hydrocarbons in addition to motor vehicles contributing significantly to the Bakersfield UCM.

To investigate the temporal trends in this potentially large source of semivolatile branched hydrocarbons, the B1/N ratios are derived from EI data using the method previously described. B1/N ratios of only C_{23} and C_{24} can be reliably determined from EI data, owing to co-elution of

other linear alkanes with B2 isomers (see Fig. 6). Extensive comparisons to speciated VOC concentrations in the region showed poor correlations of B1/N ratios to volatile tracers of known sources, such as gasoline and diesel vehicles, and natural gas production. One potential source of semivolatile hydrocarbons is the oil extraction and refining operations in the area, as Bakersfield is surrounded by numerous oil and gas fields, and two refineries are within 15 km of the sampling site. The isomer distributions of C_{21}–C_{24} hydrocarbons of the ambient Bakersfield samples are therefore compared to those of 3 crude oil samples and one motor oil (SAE 10W-30) sample. As shown in Fig. 8, the B/N ratios of the 3 crude oil samples vary by an order of magnitude. It is well known that the chemical composition of crude oil is highly variable, and the purpose of refining operations is to modify the chemical composition (relative concentrations of alkanes, alkenes, cycloalkanes, aromatics etc.) for fuel, oil, chemical feedstock or other uses. Lubricating oil, for example, has higher concentrations of cycloalkanes (also known as naphthenes) and branched alkanes than *n*-alkanes, as the viscosities of *n*-alkanes have stronger temperature dependence and increase significantly when motor engines heat up [*Gary et al.*, 2007]. While detailed characterization of the crude oil samples is beyond the scope of this work, the highly branched alkane content observed in Bakersfield is consistent with that in motor oil and one of the 3 crude oil samples analyzed. At this point, only qualitative comparisons are possible, but based on available data the high concentrations of branched alkanes in the UCM are likely related to oil extraction and/or refining operations. In the future, detailed speciation of alkane isomers in direct emissions from oil operations could be useful in quantitatively determining their importance as a source of semivolatile hydrocarbons in this area.

Modeling relative SOA formation from branched and linear alkanes

Oxidation of semivolatile alkanes has been proposed to contribute significantly to urban SOA formation. While branched isomers tend to fragment upon oxidation, their emissions are higher and are oxidized more rapidly, because of their higher volatility and greater reactivity toward OH radicals. Using the relative loss rates from CalNex LA, we formulate a simple box model to investigate the relative contributions to SOA formation from branched and linear alkanes. Based on equation (1), the ratio of SOA mass formed from branched alkanes to that from their linear isomer for a particular carbon number can be described by:

$$\frac{SOA_B}{SOA_N} = \left(\frac{B}{N}\right)_0 \left(\frac{1-e^{-k_B f_B \int [OH] dt}}{1-e^{-k_N f_N \int [OH] dt}}\right) \left(\frac{Y_B}{Y_N}\right) \qquad (3)$$

where Y_B and Y_N are the SOA mass yields for a branched alkane and a linear alkane, respectively. To the authors' knowledge, there are no existing experimental measurements of SOA yields from alkanes greater than 21 carbons. Here we calculate the theoretical SOA yields using a near-explicit gas-phase oxidation mechanism and theoretical partitioning based on work by *Jordan et al.* [2008]. We note that the SOA yields of C_{21}–C_{24} *n*-alkanes calculated from this approach are lower than those derived from extrapolating the volatility basis set parameters recommended by *Presto et al.* [2010] to this carbon number range. However, the approach by *Jordan et al.* [2008] is preferred here because the inclusion of a fragmentation mechanism is straightforward and the volatility basis set does not distinguish between different alkane isomers.

The partitioning of alkanes between gas and aerosol phase (f_B and f_N) depend critically on organic loading and temperature. For our base case simulation, we assume an organic loading of 10 μg m^{-3} and an average temperature of 293K, which is typical of ambient conditions during CalNex LA. For modeling the SOA yields Y_B and Y_N, we use a branching ratio of 0.30 for the fragmentation pathway in branched alkanes system, and assume it leads to a ketone with a

carbon number half that of the parent alkane. For linear alkanes, this branching ratio is set to 0. We assume that [OH] is constant at 2×10^6 molec cm^{-3} and perform the simulation for 8 hours, the maximum photochemical age observed in LA. Figure 9 shows the ratio of SOA mass from branched alkanes to that of linear alkanes (hereafter referred to as the BNSOA ratio) for this base case scenario. The more reactive branched alkanes form SOA earlier than linear alkanes, causing the BNSOA ratio to decrease over time. However, as shown in the contour plots in Fig. 10 and in Eqn (3), the BNSOA ratio is linear with respect to $(B/N)_0$ and is therefore a stronger function of the emission ratios than photochemical age under typical urban conditions. Also, as demonstrated in previous sections, the $(B/N)_0$ can vary by an order of magnitude depending on the source. In the range of $(B/N)_0$ observed in this work, BNSOA ratio is expected to be at least 0.5 for all carbon numbers, and can be greater than 10 in many cases. These results are qualitatively consistent with those from recent laboratory experiments and demonstrate these previously unresolved alkanes are dominant SOA precursors [*Tkacik et al.*, 2012].

Figure 11 shows the relative importance of different parameters that affect the BNSOA ratio, including gas/particle partitioning (f_B and f_N), gas-phase kinetics (k_B and k_N), SOA yields and emission ratios. Branched alkanes have lower SOA yields owing to greater extent of fragmentation. However, as a result of their higher volatilities, larger OH rate constants and higher emissions, SOA formation from branched alkanes are expected to be up to 9 times that from linear alkanes in this carbon number range. In particular, the partitioning between gas and particle phases of the alkane precursors plays an important role in determining their availability for gas-phase OH reaction, especially for C_{24}, where the difference in gas phase fractions between linear and branched isomers are the greatest. It is therefore expected that temperature

and organic loading have important effects on the relative oxidation rates through gas/particle partitioning and SOA formation.

To examine these effects, we carry out sensitivity analyses by performing the simulations at different temperatures and organic mass concentrations representing the typical range of conditions during CalNex. It is important to note that the effect of temperature and organic loading on oxidation rates is opposite to that on SOA yields. Assuming gas/particle equilibrium, increasing organic mass leads to a smaller gas-phase fraction of both the alkane precursors and their oxidation products, leading to lower effective oxidation rates and higher SOA yields simultaneously. As shown in Fig. 12a, the organic loading increases the relative contribution of branched SOA, indicating that these two effects are greater for branched alkanes than for linear alkanes. Figure 12b shows the effect of temperature on BNSOA ratio. While increasing temperature increases fractions of both branched and linear alkanes in the gas phase (f_B and f_N, respectively), it increases f_N by a larger fraction than f_B, since branched alkanes are more volatile. Owing to this shift in partitioning at higher temperatures, the relative decay of branched to linear alkanes is expected to be smaller, so the relative contribution of branched isomers to SOA is reduced. This also rules out temperature fluctuations to be the cause of the observed daytime decrease in B/N ratios of the precursor alkanes shown in Fig. 7, as higher daytime temperatures should lead to *higher* B/N ratios (of the precursor alkanes) and *lower* BNSOA ratios. Here we examine the effect of temperature on partitioning of the alkanes only, since the partitioning parameters of their oxidation products (e.g. vapor pressures, heat of vaporization) and temperature dependence of SOA yields are poorly understood.

Lastly, we used this box model to examine the effect of oxidation parameters on relative SOA formation. As expected, an increase in oxidation rate constant of branched alkane relative to that of linear alkane translates into a linear increase in BNSOA. It should be noted that the photochemical age simulated here is typical of urban conditions (3 hours). On these timescales, the effects of relative kinetics are expected to be more dominant than on longer timescales. The relative amount of fragmentation versus functionalization also determines the ratio of SOA yields, with fragmentation expected to be more significant for branched alkanes [*Lim and Ziemann*, 2009]. Here we show that the relative SOA formation vary linearly with changes in the branching ratio for the fragmentation pathway. These results imply that the uncertainties in estimating k_B and k_N (~20% difference between SRR predictions and ambient measurements) have small impacts on relative SOA contributions. On the other hand, more accurate estimates of branching between fragmentation and functionalization are needed to constrain SOA formation potentials from different alkane isomers.

Atmospheric Implications

In this work, we present detailed characterization of SVOCs observed at two different urban sites to understand the sources and processing of semivolatile alkanes. In both LA and Bakersfield samples, GC×GC analysis provides excellent separation of polar and aromatic compounds. For the aliphatic UCM, GC coupled with soft photoionization mass spectrometry, such as VUV, provides detailed characterization of alkane isomers. The unresolved complex mixture of alkane isomers was resolved by carbon number, number of rings, and, for saturated alkanes, the degree of branching. This unprecedented level of detail provides interesting insights into the photochemical processing of semivolatile hydrocarbons, which are important precursors to SOA

in the atmosphere. The ratio of branched to linear isomers for alkanes of the same carbon number decreased with photochemical processing in the LA Basin, consistent with a higher reaction rate of branched alkanes with OH radicals relative to linear alkanes. Detailed characterization of the UCM also provides information about sources, such as the odd carbon number preference and high relative concentrations of branched alkanes in the Bakersfield UCM consistent with the influences of plant wax and oil operations. Combining our speciated measurements (rate constants and emission ratios) and theoretical modeling (partitioning and SOA yields), branched alkanes are expected to contribute up to an order magnitude more to SOA formation that linear alkanes, despite lower SOA yields. The relative contributions depend strongly on their emission ratios and gas/particle partitioning for this range of volatility.

These novel measurements provide a basis to understand atmospheric processing of different hydrocarbons in the UCM, especially those from fossil fuel related sources. The ability to speciate aliphatic compounds provides important constraints on both their effective oxidation rates, and potentials to form SOA. As shown in this work, branched alkanes have higher OH reaction rates and their emissions from fossil fuel related sources can be up to an order of magnitude higher than those of linear alkanes. Since branched alkanes react more rapidly with OH radicals than linear alkanes, the ratio of their concentrations serves as an indicator for degree of processing of SVOCs. This concept is similar to using VOC ratios to estimate the gas-phase photochemical age, but is more relevant to understanding SOA formation, since oxidation of SVOCs more readily forms low-volatility material. Our simple box model demonstrates that the oxidation rates of SVOC depend strongly on the fraction in the gas phase available for OH reaction. As a result, parameters which affect partitioning, such as organic loading and

temperature, also influence the oxidation kinetics. Quantitative measurements of gas/particle partitioning are therefore crucial to understanding the oxidation of SVOCs, which is expected to be their dominant loss process in the atmosphere. Also, when using SVOCs as source tracers or to estimate photochemical age, their gas/particle partitioning must be taken into account to accurately determine the extent of their atmospheric processing.

Owing to differences in gas-phase oxidation chemistry, SOA yields depend strongly on molecular structure. Branched alkanes have a higher tendency to fragment upon oxidation, leading to more volatile products and lower SOA formation [*Lim and Ziemann*, 2009]. However, as demonstrated by our box model, oxidation of branched alkanes is expected to play a more important role in SOA formation as a result of higher emissions, faster gas-phase oxidation rate constants and higher volatility. In this work we focus our analysis on saturated alkanes. Cyclic alkanes retain the carbon backbone after ring cleavage, resulting in higher SOA yields than linear alkanes. Also, their observed emissions are greater than those of saturated alkanes. Their contributions to urban SOA formation are therefore potentially important, and accurate modeling will require a combination of speciated measurements using GC/VUV and laboratory studies into their oxidation chemistry and SOA formation mechanisms [*Lim and Ziemann*, 2009; *Tkacik et al.*, 2012].

Since SOA yields depend strongly on molecular structure, classification of organic species by volatility alone fails to fully capture SOA formation potential. Speciation by carbon number, number of rings and alkyl branching shown in this work provides detailed knowledge of both volatility and molecular structure, and hence insights into SOA formation from the UCM, the

major component in many SVOC sources. More detailed chemical characterization of SVOCs may also give crucial information about their sources. With more time-resolved samples, measurements of compounds speciated by molecular structure can be more broadly applied in factor analysis and can serve as valuable inputs for source attribution. Ultimately, despite the complexity of organic mixtures, detailed speciation is an important direction providing essential understanding of emission sources and their environmental fates.

Acknowledgements

This research was supported by the National Oceanic and Atmospheric Administration under Award No. NA10OAR4310104. The Advanced Light Source as well as K.R.W. and T.N. were supported by the Director, Office of Energy Research, Office of Basic Energy Sciences, of the U.S. Department of Energy under Contract No. DE-AC02-05CH11231. Measurements at the Advanced Light Source were also supported by the Laboratory Directed Research and Development Program of Lawrence Berkeley National Laboratory under U.S. Department of Energy Contract No. DE-AC02-05CH11231. Caldecott tunnel measurements were supported by EPA grant RD834553. The US Environmental Protection Agency through its Office of Research and Development funded and collaborated in the research described here under Contract EP-D-10-070 to Alion Science and Technology. The manuscript has not been subjected to external peer review and has not yet been cleared for publication. Mention of trade names or commercial products does not constitute endorsement or recommendation for use. The authors would like to thank Patrick Hayes, Jose Jimenez and Sally Newman for use of AMS OA and temperature data.

References

Borbon, A. et al. (2012), Emission ratios of anthropogenic VOC in northern mid-latitude megacities: observations vs. emission inventories in Los Angeles and Paris, *J. Geophys. Res.*, doi:10.1029/2012JD018235.

Dallmann, T. R., S. J. Demartini, T. Kirchstetter, S. C. Herndon, T. Onasch, E. C. Wood, and R. A. Harley (2012), On-Road Measurement of Gas and Particle Phase Pollutant Emission Factors for Individual Heavy-Duty Diesel Trucks, *Environ. Sci. Technol.*, *46*(15), 8511–8518.

Van Deursen, M., J. Beens, J. Reijenga, P. Lipman, and C. Cramers (2000), Group-Type Identification of Oil Samples Using Comprehensive Two- Dimensional Gas Chromatography Coupled to a Time-of-Flight Mass Spectrometer (GCxGC-TOF), *J. High Resol. Chromatogr.*, *23*, 507–510.

Frysinger, G. S., R. B. Gaines, L. Xu, and C. M. Reddy (2003), Resolving the unresolved complex mixture in petroleum-contaminated sediments., *Environ. Sci. Technol.*, *37*(8), 1653–1662.

Gary, J. H., G. E. Handwerk, and M. J. Kaiser (2007), *Petroleum Refining: Technology and Economics*, 5th ed., Taylor and Francis, Boca Raton.

Gentner, D. R. et al. (2012), Elucidating secondary organic aerosol from diesel and gasoline vehicles through detailed characterization of organic carbon emissions, *P. Natl. Acad. Sci. USA*, *109*(45), 18318–18323, doi:10.1073/pnas.1212272109.

Gilman, J. B. et al. (2010), Ozone variability and halogen oxidation within the Arctic and sub-Arctic springtime boundary layer, *Atmos. Chem. Phys.*, *10*(21), 10223–10236, doi:10.5194/acp-10-10223-2010.

Goldstein, A. H., and I. E. Galbally (2007), Known and unexplored organic constituents in the earth's atmosphere, *Environ. Sci. Technol.*, *41*(5), 1514–1521.

Grieshop, A. P., M. A. Miracolo, N. M. Donahue, and A. L. Robinson (2009), Constraining the volatility distribution and gas-particle partitioning of combustion aerosols using isothermal dilution and thermodenuder measurements., *Environ. Sci. Technol.*, *43*(13), 4750–4756.

Heald, C. L. et al. (2011), Exploring the vertical profile of atmospheric organic aerosol: comparing 17 aircraft field campaigns with a global model, *Atmos. Chem. Phys.*, *11*(24), 12673–12696, doi:10.5194/acp-11-12673-2011.

Hodzic, A., J. L. Jimenez, S. Madronich, M. R. Canagaratna, P. F. DeCarlo, L. Kleinman, and J. Fast (2010), Modeling organic aerosols in a megacity: potential contribution of semi-volatile and intermediate volatility primary organic compounds to secondary organic aerosol formation, *Atmos. Chem. Phys.*, *10*(12), 5491–5514, doi:10.5194/acp-10-5491-2010.

Isaacman, G. et al. (2012a), Improved resolution of hydrocarbon structures and constitutional isomers in complex mixtures using gas chromatography-vacuum ultraviolet-mass spectrometry., *Anal. Chem.*, *84*(5), 2335–2342, doi:10.1021/ac2030464.

Isaacman, G., A. W. H. Chan, T. Nah, D. R. Worton, C. R. Ruehl, K. R. Wilson, and A. H. Goldstein (2012b), Heterogeneous OH oxidation of motor oil particles causes selective depletion of branched and less cyclic hydrocarbons, *Environ. Sci. Technol.*, *46*, 10632–10640.

Isaacman, G., D. R. Worton, N. M. Kreisberg, C. J. Hennigan, A. P. Teng, S. V. Hering, A. L. Robinson, N. M. Donahue, and A. H. Goldstein (2011), Understanding evolution of product composition and volatility distribution through in-situ GC × GC analysis: a case study of longifolene ozonolysis, *Atmos. Chem. Phys.*, *11*(11), 5335–5346, doi:10.5194/acp-11-5335-2011.

Jimenez, J. L. et al. (2009), Evolution of organic aerosols in the atmosphere., *Science*, *326*(5959), 1525–1529, doi:10.1126/science.1180353.

Jordan, C. E., P. J. Ziemann, R. J. Griffin, Y. B. Lim, R. Atkinson, and J. Arey (2008), Modeling SOA formation from OH reactions with C8–C17 n-alkanes, *Atmos. Env.*, *42*(34), 8015–8026, doi:10.1016/j.atmosenv.2008.06.017.

Kwok, E. S. C., and R. Atkinson (1995), Estimation of hydroxyl radical reaction rate constants for gas-phase organic compounds using a structure-reactivity relationship: an update, *Atmos. Env.*, *29*(14), 1685–1695.

Lambe, A. T., M. A. Miracolo, C. J. Hennigan, A. L. Robinson, and N. M. Donahue (2009), Effective Rate Constants and Uptake Organic Molecular Markers in Motor Oil and Diesel Primary Radicals, *Environ. Sci. Technol.*, *43*(23), 8794–8800.

Lim, Y. B., and P. J. Ziemann (2009), Effects of molecular structure on aerosol yields from OH radical-initiated reactions of linear, branched, and cyclic alkanes in the presence of NOx., *Environ. Sci. Technol.*, *43*(7), 2328–2334.

Liu, S. et al. (2012), Secondary organic aerosol formation from fossil fuel sources contribute majority of summertime organic mass at Bakersfield, *J. Geophys. Res.*, *117*, D00V26, doi:10.1029/2012JD018170.

Mao, D., H. Van De Weghe, R. Lookman, G. Vanermen, N. De Brucker, and L. Diels (2009), Resolving the unresolved complex mixture in motor oils using high-performance liquid chromatography followed by comprehensive two-dimensional gas chromatography, *Fuel*, *88*(2), 312–318, doi:10.1016/j.fuel.2008.08.021.

Marzi, R., B. E. Torkelson, and R. K. Olson (1993), A revised carbon preference index, *Org. Geochem.*, *20*(8), 1303–1306.

Nelson, R. K., B. M. Kile, D. L. Plata, S. P. Sylva, L. Xu, C. M. Reddy, R. B. Gaines, G. S. Frysinger, and S. E. Reichenbach (2006), Tracking the Weathering of an Oil Spill with Comprehensive Two-Dimensional Gas Chromatography, *Environ. Forensics*, *7*(1), 33–44, doi:10.1080/15275920500506758.

Pankow, J., and W. Asher (2008), SIMPOL. 1: a simple group contribution method for predicting vapor pressures and enthalpies of vaporization of multifunctional organic compounds, *Atmos. Chem. Phys.*, *8*, 2773–2796, doi:10.5194/acp-8-2773-2008.

Parrish, D. D., A. Stohl, C. Forster, E. L. Atlas, D. R. Blake, P. D. Goldan, W. C. Kuster, and J. A. de Gouw (2007), Effects of mixing on evolution of hydrocarbon ratios in the troposphere, *J. Geophys. Res.*, *112*(D10S34), D10S34, doi:10.1029/2006JD007583.

Pollack, I. B. et al. (2012), Airborne and ground-based observations of a weekend effect in ozone, precursors, and oxidation products in the California South Coast Air Basin, *J. Geophys. Res.*, *117*, D00V05, doi:10.1029/2011JD016772.

Presto, A. A., C. J. Hennigan, N. T. Nguyen, and A. L. Robinson (2012), Determination of Volatility Distributions of Primary Organic Aerosol Emissions from Internal Combustion Engines Using Thermal Desorption Gas Chromatography Mass Spectrometry, *Aerosol Sci. Tech.*, *46*(10), 1129–1139, doi:10.1080/02786826.2012.700430.

Presto, A. A., M. A. Miracolo, N. M. Donahue, and A. L. Robinson (2010), Secondary organic aerosol formation from high-NOx photo-oxidation of low volatility precursors: n-alkanes, *Environ. Sci. Technol.*, *44*, 2029–2034.

Pye, H. O. T., and J. H. Seinfeld (2010), A global perspective on aerosol from low-volatility organic compounds, *Atmos. Chem. Phys.*, *10*(9), 4377–4401, doi:10.5194/acp-10-4377-2010.

Robinson, A. L., N. M. Donahue, M. K. Shrivastava, E. A. Weitkamp, A. M. Sage, A. P. Grieshop, T. E. Lane, J. R. Pierce, and S. N. Pandis (2007), Rethinking organic aerosols: semivolatile emissions and photochemical aging., *Science*, *315*(5816), 1259–1262, doi:10.1126/science.1133061.

Schauer, J., M. Kleeman, and G. Cass (1999), Measurement of emissions from air pollution sources. 2. C1 through C30 organic compounds from medium duty diesel trucks, *Environ. Sci. Technol.*, *33*(10), 1578–1587.

Schauer, J., M. Kleeman, and G. Cass (2002), Measurement of emissions from air pollution sources. 5. C1-C32 organic compounds from gasoline-powered motor vehicles, *Environ. Sci. Technol.*, *36*, 1169–1180.

Tkacik, D. S., A. A. Presto, N. M. Donahue, and A. L. Robinson (2012), Secondary organic aerosol formation from intermediate-volatility organic compounds: cyclic, linear, and branched alkanes., *Environ. Sci. Technol.*, *46*(16), 8773–8781, doi:10.1021/es301112c.

Ventura, G. T., F. Kenig, C. M. Reddy, G. S. Frysinger, R. K. Nelson, B. Van Mooy, and R. B. Gaines (2008), Analysis of unresolved complex mixtures of hydrocarbons extracted from Late Archean sediments by comprehensive two-dimensional gas chromatography (GC×GC), *Org. Geochem.*, *39*(7), 846–867, doi:10.1016/j.orggeochem.2008.03.006.

Vogt, L., T. Gröger, and R. Zimmermann (2007), Automated compound classification for ambient aerosol sample separations using comprehensive two-dimensional gas chromatography-time-of-flight mass spectrometry., *J. Chromatogr. A*, *1150*(1-2), 2–12, doi:10.1016/j.chroma.2007.03.006.

Wang, F. C.-Y., K. Qian, and L. A. Green (2005), GCxMS of diesel: a two-dimensional separation approach., *Anal. Chem.*, *77*(9), 2777–2785, doi:10.1021/ac0401624.

Williams, B. J., A. H. Goldstein, N. M. Kreisberg, and S. V Hering (2010a), In situ measurements of gas/particle-phase transitions for atmospheric semivolatile organic compounds., *P. Natl. Acad. Sci. USA*, *107*(15), 6676–6681, doi:10.1073/pnas.0911858107.

Williams, B. J., A. H. Goldstein, N. M. Kreisberg, S. V. Hering, D. R. Worsnop, I. M. Ulbrich, K. S. Docherty, and J. L. Jimenez (2010b), Major components of atmospheric organic aerosol in southern California as determined by hourly measurements of source marker compounds, *Atmos. Chem. Phys.*, *10*(23), 11577–11603, doi:10.5194/acp-10-11577-2010.

Worton, D. R., N. M. Kreisberg, G. Isaacman, A. P. Teng, C. McNeish, T. Górecki, S. V. Hering, and A. H. Goldstein (2012), Thermal Desorption Comprehensive Two-Dimensional Gas Chromatography: An Improved Instrument for In-Situ Speciated Measurements of Organic Aerosols, *Aerosol Sci. Tech.*, *46*(4), 380–393, doi:10.1080/02786826.2011.634452.

Zhang, Q. et al. (2007), Ubiquity and dominance of oxygenated species in organic aerosols in anthropogenically-influenced Northern Hemisphere midlatitudes, *Geophys. Res. Lett.*, *34*, L13801, doi:10.1029/2007GL029979.

Zhao, Y. et al. (2012), Major components of summer-time organic aerosol in Bakersfield, CA, *J. Geophys. Res.*, submitted.

Table 1. Gas-phase OH reaction rate constants of linear (k_N) and branched (k_B) alkanes calculated by structure-reactivity relationships (SRR) [*Kwok and Atkinson*, 1995], the rate ratios (k_B/k_N) calculated from SRR and observed in ambient LA samples. The uncertainties in observed rate ratios are derived from the standard deviations in the regressions shown in Fig. 5. See Appendix C in the Supplementary Material for derivation of k_{B1} from EI data.

Carbon Number	k_N (10^{-11} cm^3 $molec^{-1}$ sec^{-1}) from SRR	k_B (10^{-11} cm^3 $molec^{-1}$ sec^{-1}) from SRR	k_{B1}/k_N (SRR)	k_{B2}/k_N (SRR)	k_B/k_N observed (from VUV data)	k_{B1}/k_N observed (from EI data)
21	2.66	2.88	1.08	1.01	1.21 ± 0.47	
22	2.80	3.03	1.08	1.01	1.31 ± 0.48	1.32
23	2.94	3.17	1.08	1.01	1.25 ± 0.13	1.12
24	3.08	3.31	1.07	1.01	1.35 ± 0.50	1.14

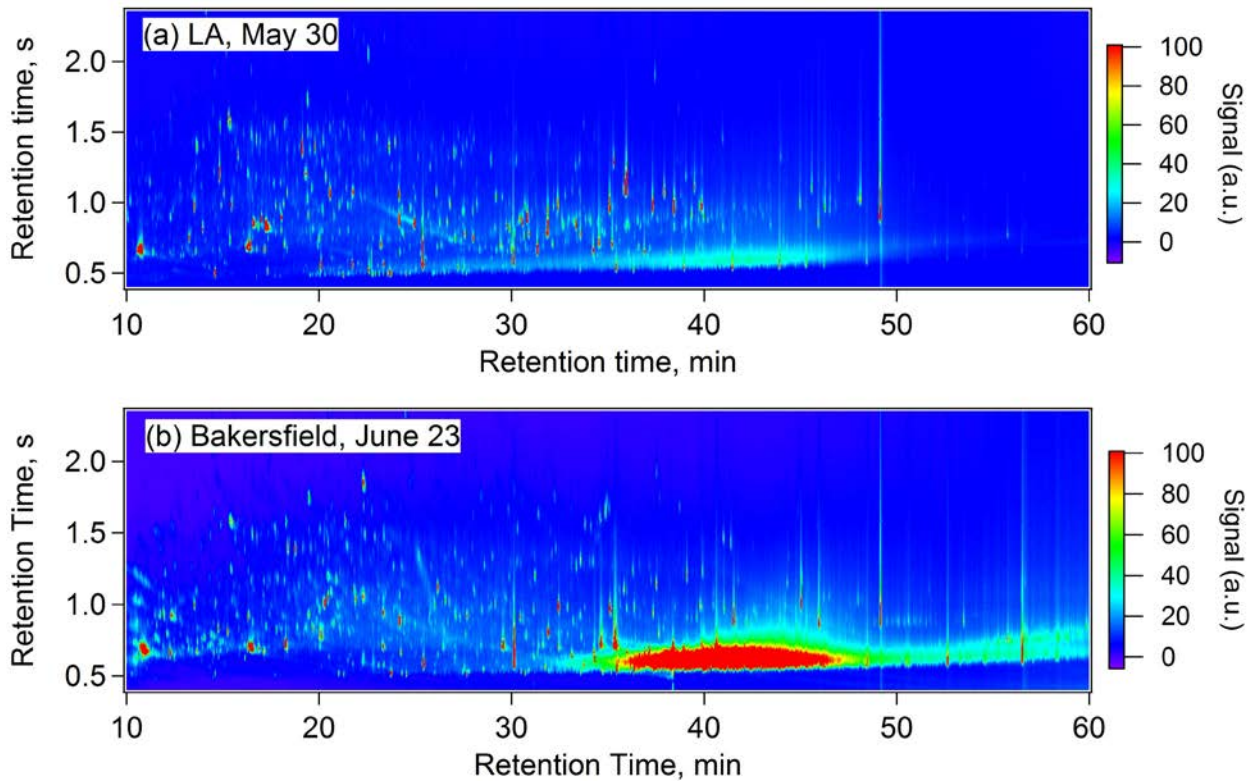

Figure 1. Total Ion Chromatogram of (a) LA sample (May 30) and (b) Bakersfield sample (June 23). The unresolved complex mixture (UCM) of aliphatic hydrocarbons, between first-dimension retention times of 30 and 50 minutes, is evident in both samples.

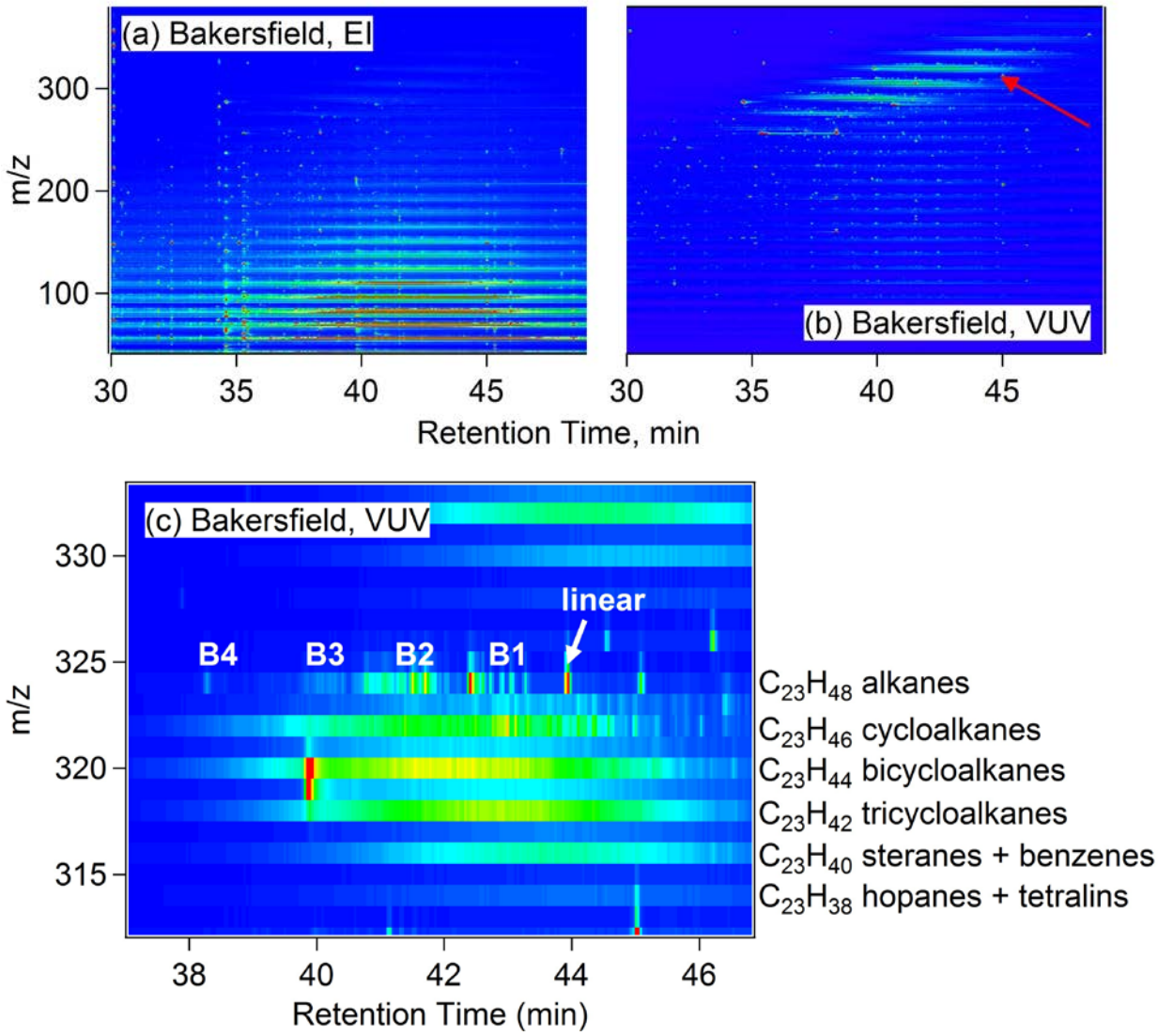

Figure 2. GC×MS plots of UCM in Bakersfield sample (June 23) under (a) EI and (b) VUV ionization. (a) Under electron impact, strong fragmentation causes most of the signal to fall on the same fragment $C_xH_y^+$ ions, as delineated by horizontal lines along a few select *m/z*'s. (b) Under VUV, molecular ions are retained, and cluster by carbon number in a GC×MS plot. One such cluster denoted by the red arrow is expanded into Panel (c). Within each carbon number, aliphatic hydrocarbons were resolved by number of rings (by molecular weight) and by degree of branching for acyclic alkanes, denoted by B*x*, where *x* is the number of alkyl branches.

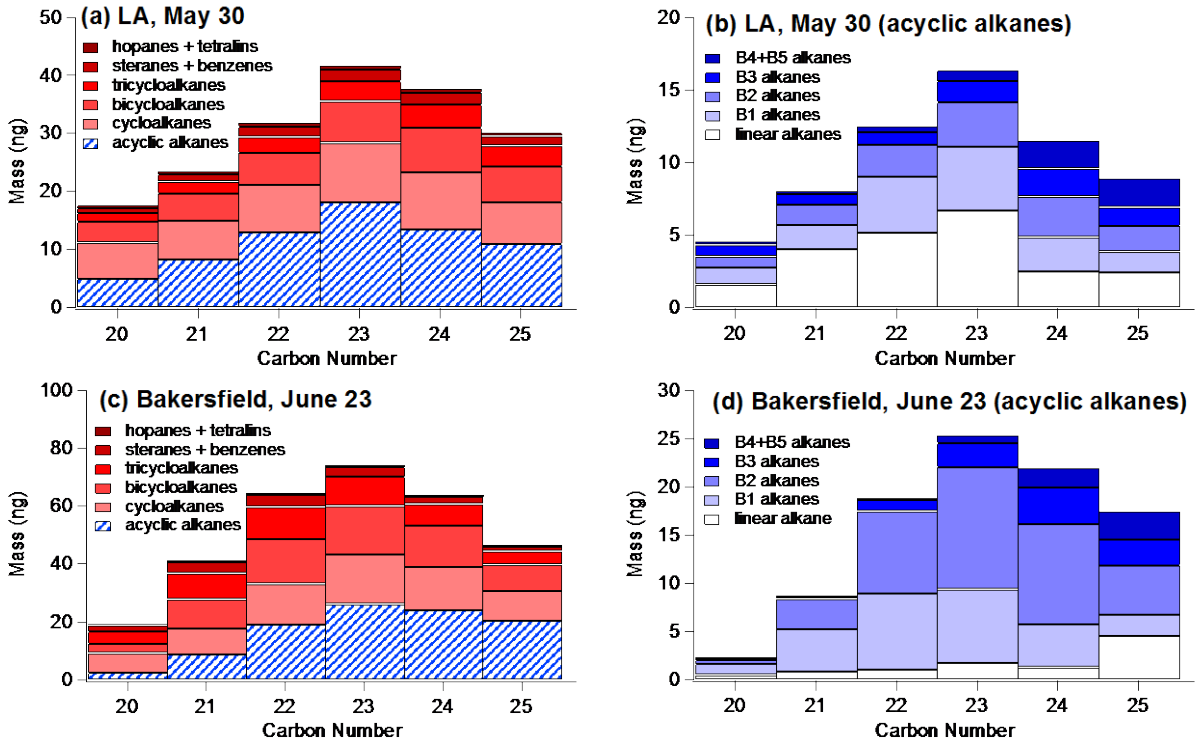

Figure 3. Distribution of alkane isomers in LA (May 30) and Bakersfield (June 23) samples. In panels (a) and (c), isomers are grouped by N_{DBE}, ranging from 0 (acyclic) to 6 (hopanes and tetralins). In panels (b) and (d), the signals include only those of acyclic (linear and branched) alkanes. While the distributions among different N_{DBE} in LA and Bakersfield are similar, the branched acyclic alkanes are more abundant relative to linear alkanes in Bakersfield than in LA.

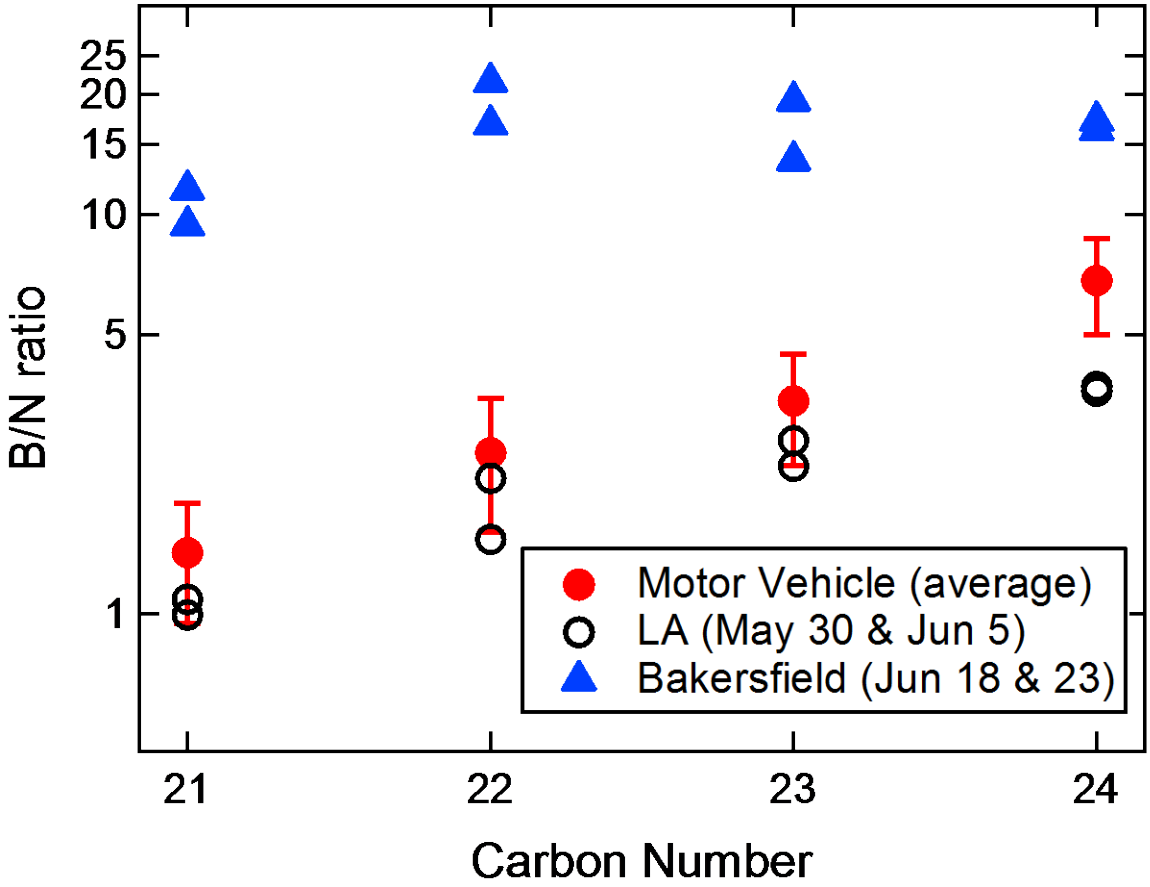

Figure 4. Ratios of branched to linear alkanes (B/N) of CalNex ambient samples and Caldecott tunnel samples ("Motor Vehicle") analyzed using VUV photoionization. For the motor vehicle samples, the B/N ratios shown here averaged over all 7 samples, and the error bars represent the standard deviations in the 7 samples.

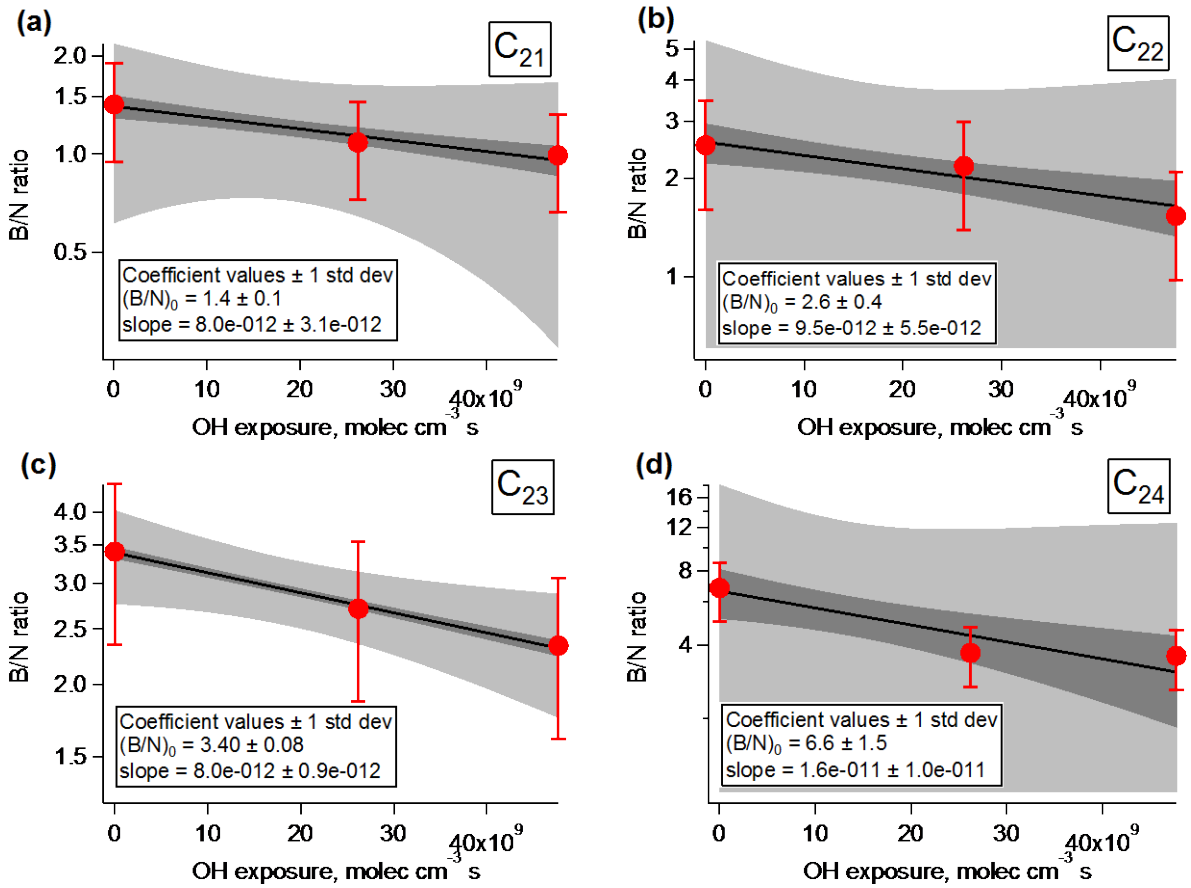

Figure 5. Ratios of branched to linear alkanes (B/N) of LA samples measured by VUV as a function of OH exposure. The B/N ratios at zero OH exposure are taken to be those from the tunnel samples of fresh motor vehicle exhaust. OH exposure for the LA samples were calculated using the ratio of 1,2,4-TMB to benzene [*Borbon et al.*, 2012]. The black lines represent the best-fit lines to equation (1), and the fitted coefficients are shown in Table 1. The dark grey and light grey shaded areas represent the 68% and 95% confidence intervals of the regressions, respectively.

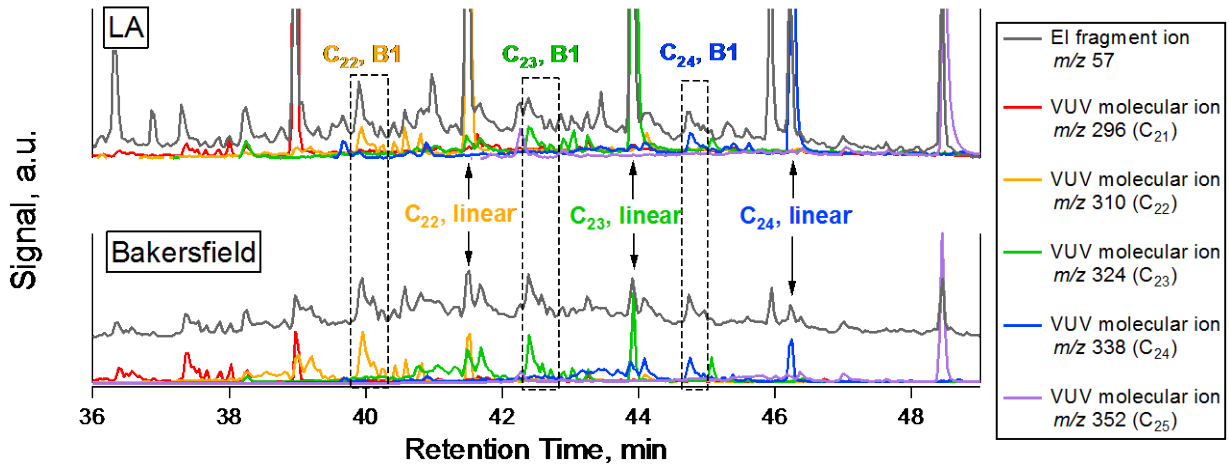

Figure 6. Extracted ion chromatograms of *m/z* 57 under EI (dark grey) and molecular ions of alkanes under VUV (all other colors). For each molecular ion, the latest eluting peak represents the linear alkane. Under EI, *m/z* 57 represents the $C_4H_9^+$ ion, the most abundant fragment ion of high molecular weight alkanes. The EI *m/z* 57 trace show identical peak shapes to the molecular ion traces where the B1 isomers elute (denoted by boxes with dashed lines). Linear isomers (denoted by arrows) coelute with a B2 isomer of a higher carbon number, but for C_{23}–C_{24} in Bakersfield samples, and C_{22}–C_{24} in the LA samples, the contributions of B2 isomers are expected to be less than 15%. The ratio of B1 to linear isomers (B1/N) for each carbon number can therefore be estimated from the *m/z* 57 signal under EI.

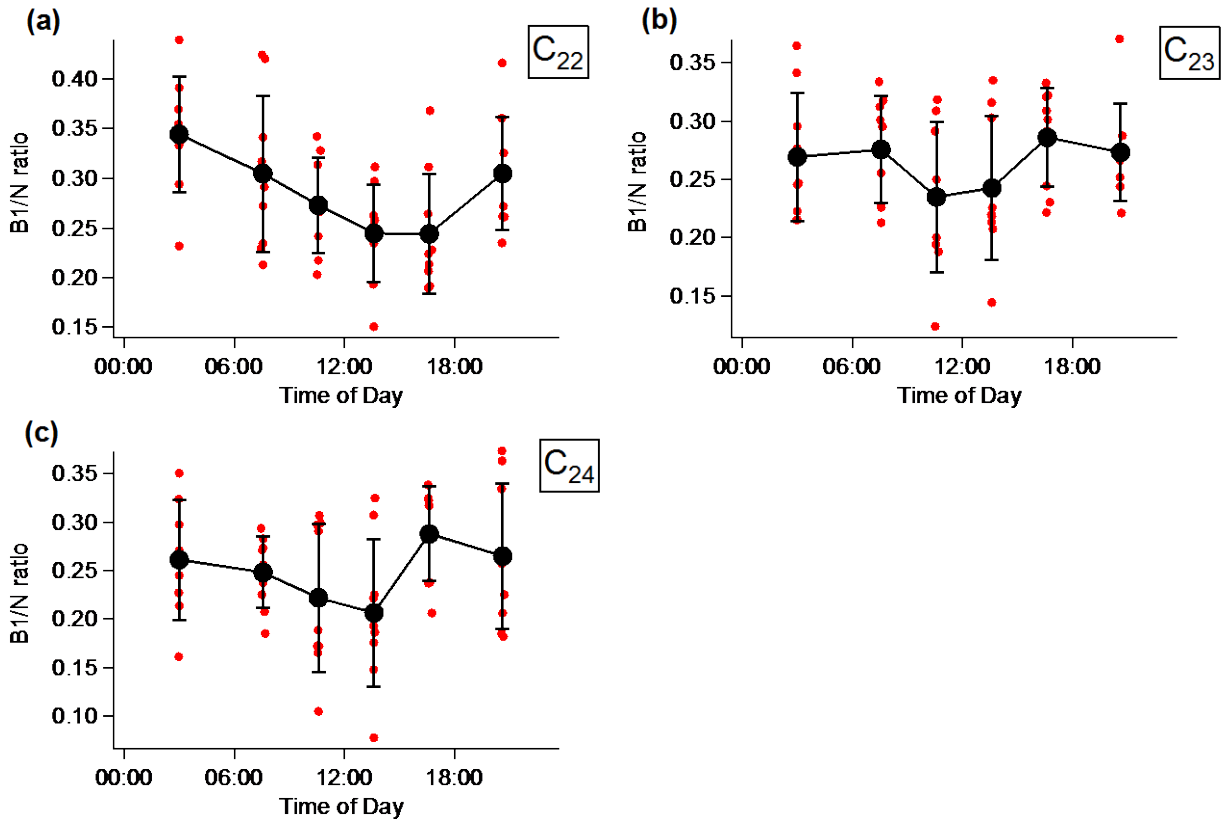

Figure 7. Diurnal profiles of B1/N ratios. The minima of B1/N ratios occur between late morning and early afternoon local time, consistent with maximum photochemical activity.

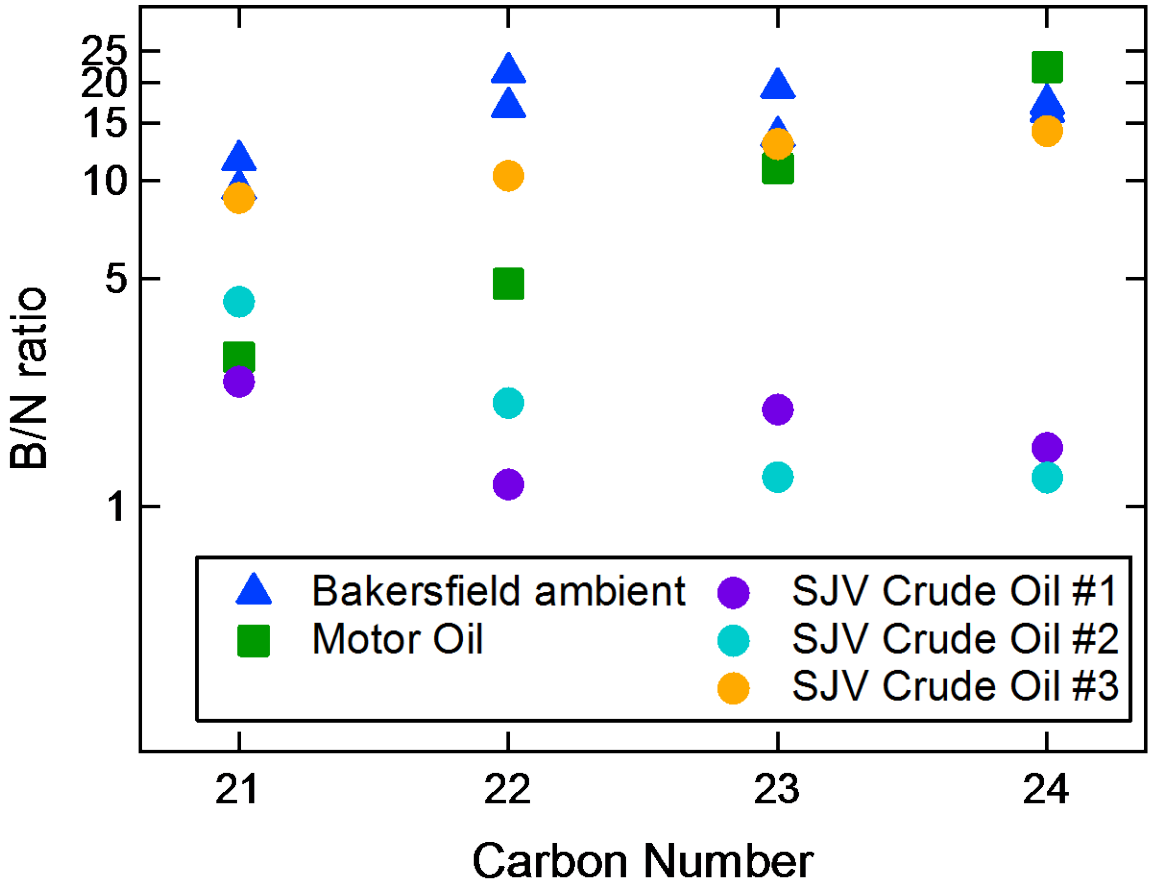

Figure 8. Ratios of branched to linear alkanes (B/N) of ambient Bakersfield samples, 10W-30 motor oil and 3 samples of crude oil extracted and/or processed in the San Joaquin Valley (SJV). Among all the samples analyzed in this work, the B/N ratios of motor oil and one SJV crude oil sample (sample 3) approach those in Bakersfield, suggesting the source of these hydrocarbons is related to oil operations in the area.

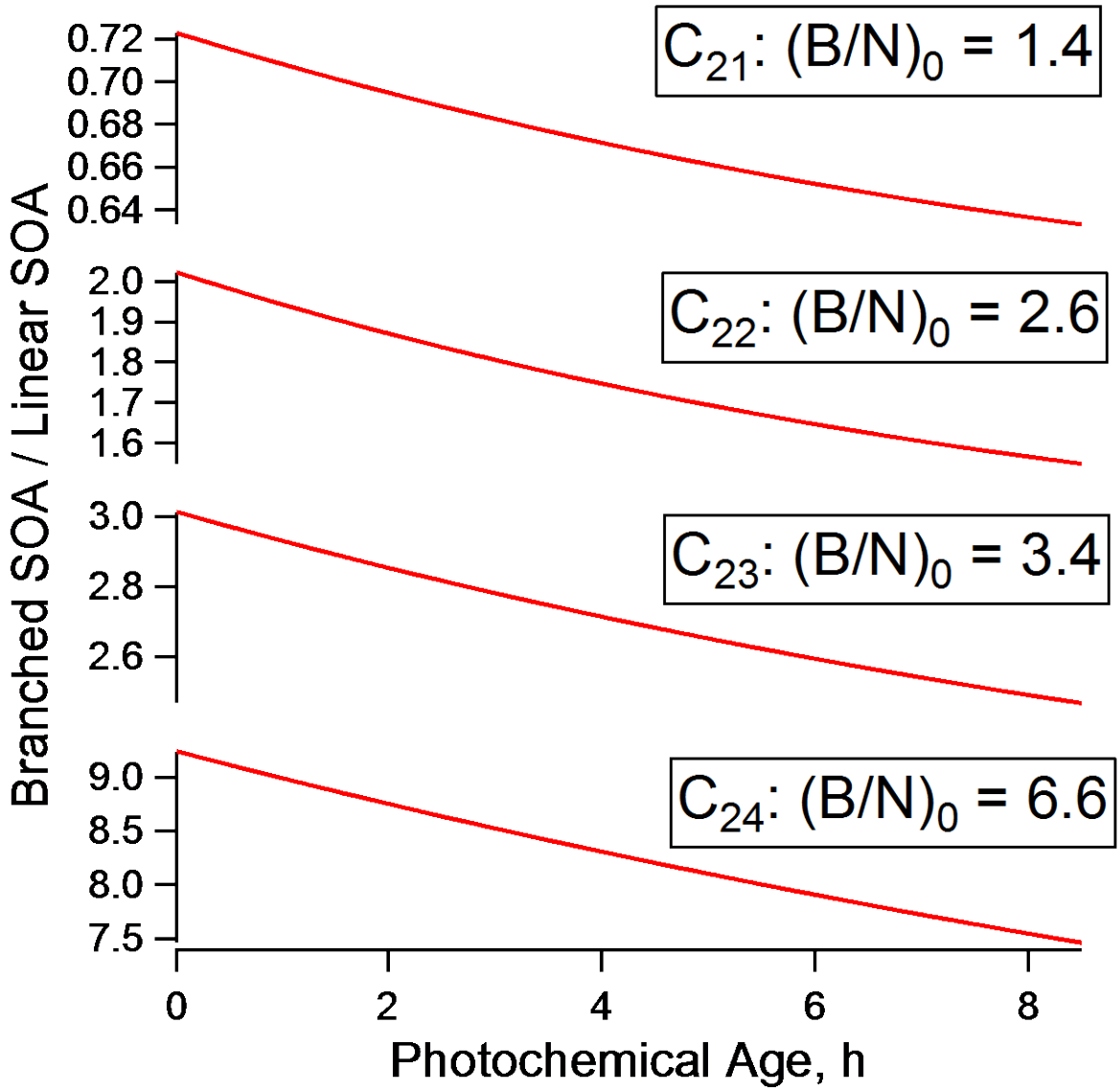

Figure 9. Base case simulation for simple box model. The mathematical equation is described by Eqn (3). For this simulation, the values for $(B/N)_0$ and k_B were derived from CalNex data summarized in Table 1. SOA yields were calculated using the oxidation mechanism from *Jordan et al.*, [2008], assuming 0.3 of reacted hydrocarbon fragments upon oxidation. The temperature of 293K and organic loading is 10 μg m^{-3}, which are typical of conditions during CalNex LA. [OH] is assumed to be constant at 2×10^6 molec cm^{-3}.

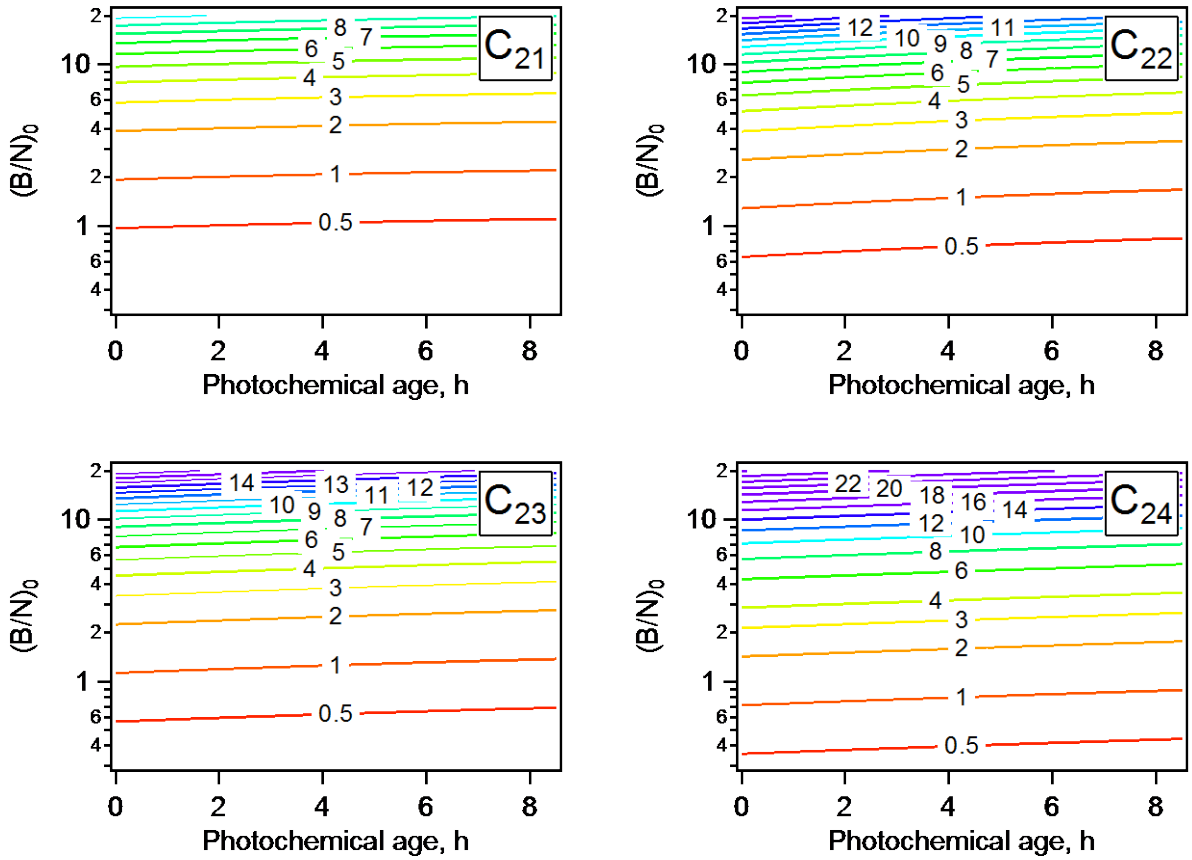

Figure 10. Contour plots of BNSOA (ratio of total SOA formation from branched alkanes to that from linear alkanes) as a function of photochemical age and emission ratios $(B/N)_0$. Simulations are carried out for the range of $(B/N)_0$ observed in this work (see Figs. 4 and 8). The contour lines are almost horizontal, indicating a stronger dependence on $(B/N)_0$ than on photochemical age. This is a result of the linear dependence of BNSOA on $(B/N)_0$ (see Eqn (3)) and wide range of $(B/N)_0$ observed.

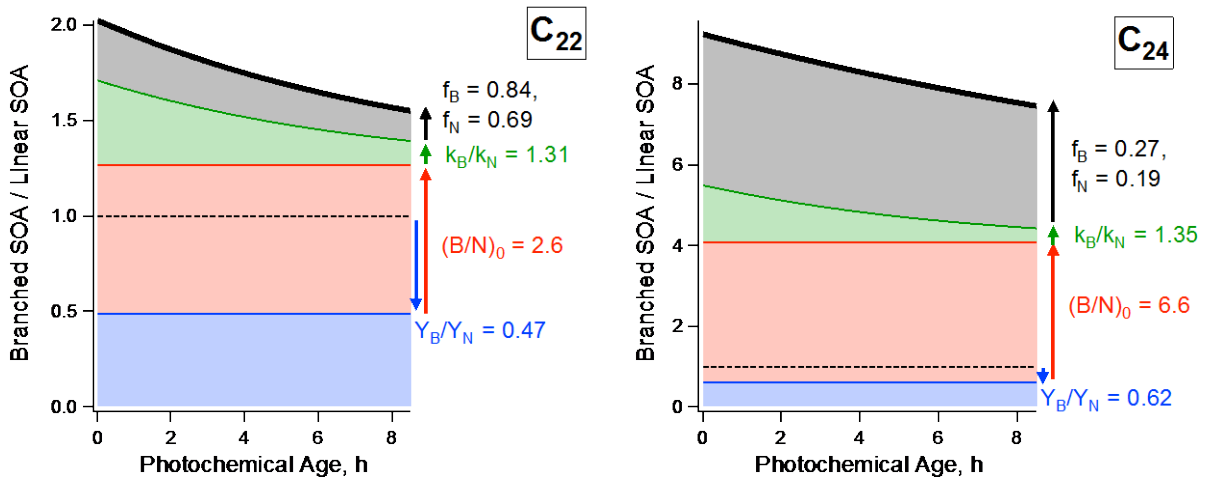

Figure 11. Effect of including various factors into determining relative SOA formation. The dotted line denotes equal SOA formation between all branched isomers and the linear alkane (BNSOA = 1). The blue line and arrow denote lowering SOA yields of branched isomers as a result of fragmentation (0.3 in this base case). The red line and arrow denote including a higher emission ratio of branched alkanes, derived from motor vehicle samples (see Fig. 4). The green line and arrow denote accounting for the differences in gas-phase oxidation rate constants, assuming all SVOCs are in the gas phase. Lastly, accounting for gas/particle partitioning results in the black line, which represents the base case scenario. The gas phase fractions (f_N and f_B) are calculated for a temperature of 293K and organic loading of 10 µg m^{-3}.

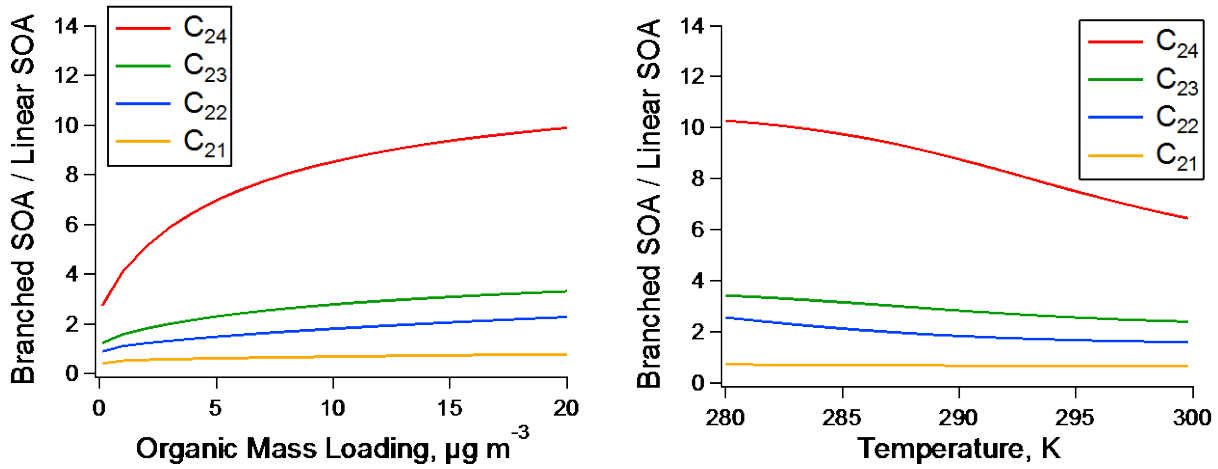

Figure 12. Effect of varying partitioning parameters on relative SOA formation. The range of organic mass loading and temperature simulated here is consistent with conditions during CalNex LA. The photochemical age for these simulations is 3 hours, at an average [OH] of 2×10^6 molec cm^{-3}. Effects of temperature on SOA yields are not taken into account, as the heat of vaporization of oxidation products are poorly understood.

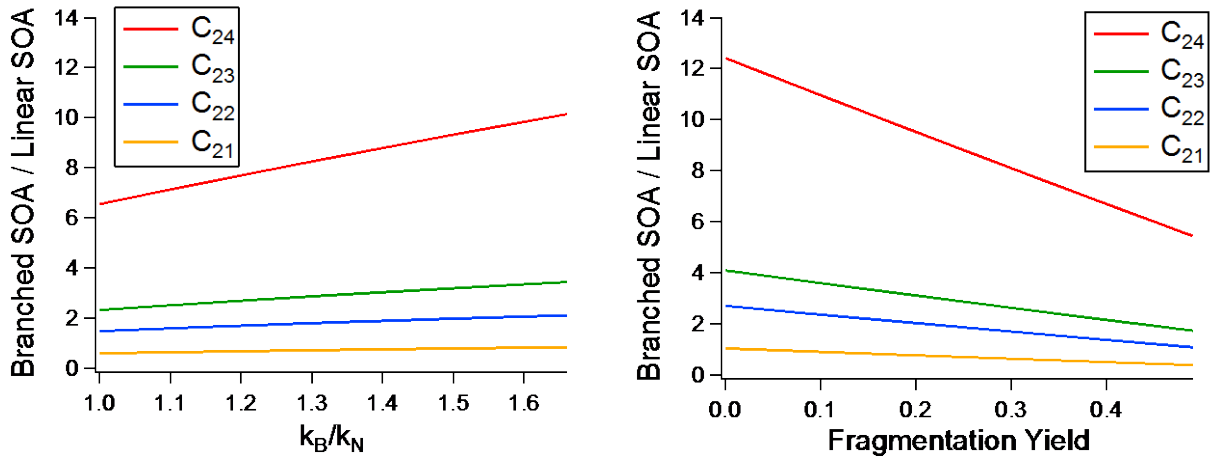

Figure 13. Effect of rate constants and fragmentation branching on relative SOA formation. The fragmentation yield is molar stoichiometric yield of the fragmentation product, which is assumed to be a ketone with half the carbon number as the parent alkane. All other parameters are kept the same as in the base case simulation (see Fig. 9).

This document was prepared as an account of work sponsored by the United States Government. While this document is believed to contain correct information, neither the United States Government nor any agency thereof, nor the Regents of the University of California, nor any of their employees, makes any warranty, express or implied, or assumes any legal responsibility for the accuracy, completeness, or usefulness of any information, apparatus, product, or process disclosed, or represents that its use would not infringe privately owned rights. Reference herein to any specific commercial product, process, or service by its trade name, trademark, manufacturer, or otherwise, does not necessarily constitute or imply its endorsement, recommendation, or favoring by the United States Government or any agency thereof, or the Regents of the University of California. The views and opinions of authors expressed herein do not necessarily state or reflect those of the United States Government or any agency thereof or the Regents of the University of California.